AGU PUBLICATIONS

JGR

Journal of Geophysical Research: Space Physics

RESEARCH ARTICLE
10.1002/2014JA020807

**Key Points:**
- Global determination of ionospheric and plasmaspheric electron contents
- Ionosphere and plasmasphere study for low solar and geomagnetic activity
- Analysis of the fractional contribution of the ionosphere to TEC

**Correspondence to:**
G. González-Casado,
Guillermo.gonzalez@upc.edu

**Citation:**
González-Casado, G., J. M. Juan, J. Sanz, A. Rovira-Garcia, and A. Aragon-Angel (2015), Ionospheric and plasmaspheric electron contents inferred from radio occultations and global ionospheric maps, *J. Geophys. Res. Space Physics*, *120*, 5983–5997, doi:10.1002/2014JA020807.

Received 10 NOV 2014
Accepted 1 JUL 2015
Accepted article online 4 JUL 2015
Published online 29 JUL 2015

# Ionospheric and plasmaspheric electron contents inferred from radio occultations and global ionospheric maps

**G. González-Casado[1], J. M. Juan[2], J. Sanz[3], A. Rovira-Garcia[3], and A. Aragon-Angel[4]**

[1]Departament de Matemàtica Aplicada 2, Universitat Politècnica de Catalunya, Barcelona, Spain, [2]Departament de Física Aplicada, Universitat Politècnica de Catalunya, Barcelona, Spain, [3]Departament de Matemàtica Aplicada 4, Universitat Politècnica de Catalunya, Barcelona, Spain, [4]Institute for the Protection and Security of the Citizen, European Commission Joint Research Centre, Ispra, Italy

**Abstract** We introduce a methodology to extract the separate contributions of the ionosphere and the plasmasphere to the vertical total electron content, without relying on a fixed altitude to perform that separation. The method combines two previously developed and tested techniques, namely, the retrieval of electron density profiles from radio occultations using an improved Abel inversion technique and a two-component model for the topside ionosphere plus protonosphere. Taking measurements of the total electron content from global ionospheric maps and radio occultations from the Constellation Observing System for Meteorology, Ionosphere, and Climate/FORMOSAT-3 constellation, the ionospheric and plasmaspheric electron contents are calculated for a sample of observations covering 2007, a period of low solar and geomagnetic activity. The results obtained are shown to be consistent with previous studies for the last solar minimum period and with model calculations, confirming the reversal of the winter anomaly, the hemispheric asymmetry of the semiannual anomaly, and the existence in the plasmasphere of an annual anomaly in the South American sector of longitudes. The analysis of the respective fractional contributions from the ionosphere and the plasmasphere to the total electron content shows quantitatively that during the night the plasmasphere makes the largest contribution, peaking just before sunrise and during winter. On the other hand, the fractional contribution from the ionosphere reaches a maximum value around noon, which is nearly independent of season and geomagnetic latitude.

## 1. Introduction

Analysis of the electron content in the ionosphere-plasmasphere system is of chief interest for applications related to radio navigation and for the climatological analysis of the thermosphere and its interplay with both the lower atmosphere and the upper magnetosphere. Global ionospheric maps (GIMs) of the total electron content (TEC), produced regularly by the International Global Navigation Satellite Systems (GNSS) service (IGS) for more than a decade, have been used to separate the ionosphere and plasmasphere contribution to the TEC at a local scale by direct comparison with collocated measurements from ionosonde data or incoherent scatter radar observations [e.g., *Belehaki et al.*, 2004; *Mosert et al.*, 2007; *Meza et al.*, 2008; *Makarevich and Nicholls*, 2013]. In such studies, the residuals of the comparison are assumed to provide an estimate of the plasmaspheric electron content. A similar approach has been followed in global studies based on satellite measurements of the ionospheric electron content taken at a fixed altitude [e.g., *Jee et al.*, 2010; *Klimenko et al.*, 2014].

Alternatively, global studies have been performed to obtain simultaneous measurements of the ionospheric and plasmaspheric electron contents, using nearly zenithal observations gathered by the precise orbit determination (POD) antennae on board satellite missions to calculate the plasmaspheric contribution to the TEC. In particular, this approach has been applied to the Jason 1 satellite observations [*Yizengaw et al.*, 2008; *Lee et al.*, 2013] and for the Constellation Observing System for Meteorology, Ionosphere, and Climate (COSMIC)/FORMOSAT-3 (CF3) constellation [*Pedatella and Larson*, 2010; *Pedatella et al.*, 2011]. However, POD observations need to be nearly vertical to minimize the impact of the obliquity factor on the results, which in the case of CF3 satellites causes the corresponding measurements of the plasmaspheric electron content to be severely affected by multipath errors because of the antenna orientation. Additionally, leveling biases (between code and carrier phase measurements) and receiver differential code biases mean that extensive

modeling and careful analysis are required to obtain reliable results. In the case of the Jason 1 satellite, an additional complication is that the measurements are affected by a systematic bias that can reach values of 5 total electron content units (1 TECU = $10^{16}$ el $m^{-2}$) [*Jee et al.*, 2010].

Despite all these difficulties, the significance of the plasmasphere contribution to the TEC has been recognized for more than a decade [e.g., *Lunt et al.*, 1999; *Gulyaeva et al.*, 2002]. Current estimates of this contribution range from 10–20%, during the day and in normal conditions of solar and geomagnetic activities, to 50–60% or even more, during the night when the electron density in the *F* region is at its lowest [*Yizengaw et al.*, 2008; *Pedatella et al.*, 2011; *Nanan et al.*, 2012; *Lee et al.*, 2013; *González-Casado et al.*, 2013]. Hence, it is of great interest to develop a methodology to quantify on a global scale, easily and accurately, the electron content in the ionosphere and the plasmasphere. Radio occultation (RO) of Global Positioning System (GPS) receivers on board low Earth orbit (LEO) satellites can be used to determine electron density profiles for altitudes below the LEO. In particular, the dense coverage in longitude, latitude, and time of the CF3 mission makes this constellation of satellites a powerful tool for retrieving all-time all-weather ionospheric information [*Schreiner et al.*, 2007]. On the basis of RO measurements from CF3 satellites, the present study is aimed to investigate an accurate method that does not rely on the LEO satellite altitude, $h_{LEO}$, to derive the distinct contributions of the ionosphere and the plasmasphere to the TEC.

The so-called upper transition height (UTH), defined as the altitude where the densities of $O^+$ and $H^+$ are equal, is conventionally used as a characteristic altitude marking the transition from the ionosphere to the plasmasphere. In this sense, the populations of $O^+$ and $H^+$ ions are considered to trace the ionospheric and plasmaspheric regions, respectively. The ionosphere-plasmasphere system is known to be subject to substantial variations depending on solar activity, local time (LT), season of the year, and geomagnetic activity. Hence, the UTH values may span a wide range of altitudes, of several hundreds of kilometers [*Yue et al.*, 2010; *González-Casado et al.*, 2013; *Aponte et al.*, 2013]. The strategy proposed in the present study is based on estimating the topside ionosphere density of $O^+$ and $H^+$ to derive the ionospheric and plasmaspheric electron contents without using a given altitude to separate them. Consequently, the resulting method does not require explicit knowledge of the location of the boundary between the ionosphere and the plasmasphere.

The structure of the paper is as follows. In section 2, we present the methodology to extract, from ground measurements of vertical total electron content (VTEC), the distinct contributions arising from the ionosphere and the plasmasphere. Section 3 gives details of the data sample used in the present study, corresponding to a period of time of quite low solar and geomagnetic activity, part of the last solar minimum. The method is assessed using this data sample in section 4, where the LT variations in the ionosphere-plasmasphere system during the March equinox and the June and December solstices are analyzed and compared with previous studies. The fractional ionospheric electron content is specifically studied in section 5. First, in section 5.1, the results derived with our methodology are validated by direct comparison with the predictions from a two-layer ionosphere-plasmasphere model currently used in GNSS precise positioning applications. Second, in section 5.2, seasonal, latitudinal, and LT variations of the fractional ionospheric electron content shown by our data sample are examined in more detail. Finally, our conclusions are summarized in section 6.

## 2. Methodology for the Derivation of the Electron Content in the Ionosphere and the Plasmasphere

The Abel transform inversion has been the usual technique to retrieve electron density profiles from ROs under the assumption of local spherical symmetry of the electron density [e.g., *Rocken et al.*, 2000]. When compared with ionosonde measurements of the $F_2$ layer peak density, the reported discrepancies of the profiles derived by means of the classical Abel inversion vary from 20 to 40% [*Aragon-Angel et al.*, 2010, 2011]. However, an alternative and more precise derivation of the electron density profile from an RO can be achieved using the improved Abel transform (IAT) introduced by *Hernández-Pajares et al.* [2000], a method that does not assume local spherical symmetry during the inversion process. Indeed, the addition of information about horizontal gradients of the VTEC allowed by the separability assumption in the IAT method improves the results of the inversion procedure, reducing the discrepancies with ionosonde measurements by about 35% with regard to the classical Abel inversion [*Garcia-Fernandez et al.*, 2003; *Aragon-Angel et al.*, 2010, 2011].

In the IAT method, the electron density, $N_e(\lambda, \varphi, h)$, is expressed as the product of a shape function *F(h)* that describes the height ($h$) dependency of $N_e$ times the externally provided VTEC at the requested geographical longitude and latitude, $\lambda$ and $\varphi$, respectively,

$$N_e(\lambda, \varphi, h) = \mathrm{VTEC}(\lambda, \varphi) \cdot F(h)\,, \tag{1}$$

where the profile $F(h)$ is the unknown to be solved while the VTEC data are obtained from measurements by ground receivers.

The simplified topside ionosphere plus protonosphere (STIP) model function [*González-Casado et al.*, 2013],

$$F_{\mathrm{ext}}(h) = A \exp\left(-h/h_s\right) + B\,, \tag{2}$$

will be used to fit the RO-retrieved profile $F_{\mathrm{RO}}(h)$ derived by means of the IAT method. The fit will be done in a range of altitudes starting above the $F_2$ peak altitude (hereafter, the minimum altitude used in the fits will be indicated by $h_{\mathrm{ext}}$) and ending a few kilometers below the LEO satellite altitude $h_{\mathrm{LEO}}$. This altitude range typically goes from 400 to 700 km and, in the following, will be referred to for simplicity as the topside ionosphere region (TIR). The STIP model is based on separating the electron density in the TIR into the sum of two terms representing the density of the $O^+$ and $H^+$ ions, respectively. The first term on the right-hand side of equation (2) describes the exponentially decaying abundance of the $O^+$ ion, with $h_s$ standing for the corresponding vertical scale height and $A$ being a proportionality factor that determines the magnitude of the ionospheric electron density compared to the second term, $B$, representing the $H^+$ ion density in the TIR, where such density can be reasonably approximated to a constant [see *González-Casado et al.*, 2013]. Thus, in equation (2) the exponential term represents the topside ionospheric electron density while the parameter $B$ describes the bottomside plasmaspheric electron density. The STIP model function has been shown to provide an accurate representation of the electron density in the TIR, significantly improving the fit to RO-retrieved electron density profiles in comparison with other classical model functions (Chapman, Epstein, or single exponential functions) [*González-Casado et al.*, 2013]. The minimum altitude used in the fits, $h_{\mathrm{ext}}$, must be higher than the altitude of the $F_2$ layer peak and not too close, in order to ensure that the exponential term on the right-hand side of equation (2) provides a good representation of the decaying abundance of $O^+$ in the TIR [*González-Casado et al.*, 2013]. Moreover, $h_{\mathrm{ext}}$ must be significantly separated from the maximum altitude used in the fit (close to $h_{\mathrm{LEO}}$) to ensure that a sufficiently large region belonging to the topside ionosphere has been used in the fits. A good compromise between these two requirements is normally found when the difference between the value of $h_{\mathrm{ext}}$ and the altitude of the $F_2$ layer peak for a particular RO is set to be approximately 2 times $h_s$.

After deriving the best fit parameters of equation (2) to a given RO-retrieved profile $F_{\mathrm{RO}}(h)$, the corresponding exponential term (or equivalently, the difference $F_{\mathrm{ext}}(h) - B$) is used to extrapolate the altitude variation of the ionospheric electron density above $h_{\mathrm{ext}}$. Figure 1 illustrates the process by showing an example of the initial $F_{\mathrm{RO}}(h)$ profile retrieved from an RO and the resulting exponential curve used to extrapolate the ionospheric electron density toward altitudes higher than $h_{\mathrm{LEO}}$. The extrapolation should end at an altitude where the $O^+$ density vanishes. But in practice, extrapolating with an infinite upper limit yields a very small difference in the result (see Appendix A), because the vertical scale height of the exponentially decaying ionospheric electron density is, typically, not greater than a few hundreds of kilometers. Consequently, the ionospheric electron content, $\mathrm{EC}_{\mathrm{ion}}$, is calculated according to the following expression:

$$\mathrm{EC}_{\mathrm{ion}}(\lambda, \varphi) = \mathrm{VTEC}(\lambda, \varphi) \left[ \int_{h_0}^{h_{\mathrm{ext}}} F_{\mathrm{RO}}(h)\, \mathrm{d}h + h_s A \exp\left(-h_{\mathrm{ext}}/h_s\right) \right], \tag{3}$$

where $h_0$ is the minimum altitude sampled by the RO (typically around 100 km) and the term added to the integral in the expression between brackets provides the topside ionosphere contribution to $\mathrm{EC}_{\mathrm{ion}}$ (see Appendix A and equation (A1)).

Finally, assuming that the VTECs can be split into the contributions from the plasmasphere and ionosphere, the corresponding electron content from the plasmasphere at a given location, $\mathrm{EC}_{\mathrm{pl}}(\lambda, \varphi)$, is immediately derived from equation (3) as

$$\mathrm{EC}_{\mathrm{pl}}(\lambda, \varphi) = \mathrm{VTEC}(\lambda, \varphi) - \mathrm{EC}_{\mathrm{ion}}(\lambda, \varphi)\,. \tag{4}$$

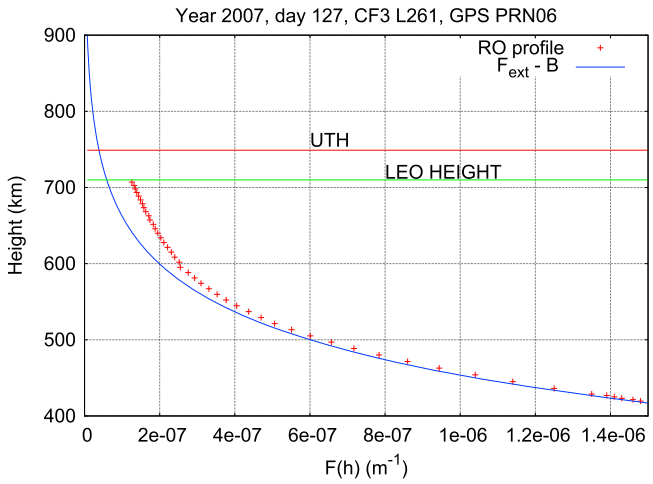


**Figure 1.** An example of the extrapolation strategy used to calculate $EC_{ion}$. Red crosses: a particular RO-retrieved shape function using the IAT method. Blue solid line: the exponential term (representing the ionospheric contribution) that has been used to calculate $EC_{ion}$ after the best fit achieved for the particular RO profile using the STIP model function $F_{ext}(h)$. The red and green horizontal lines indicate, respectively, the UTH derived from the best fit STIP model and the height of the CF3 satellite.

Further, recalling that the expression between brackets in equation (3) is equal to the fractional contribution of the ionosphere to the VTEC,

$$\mathrm{ION}_f = \frac{\mathrm{EC}_{\mathrm{ion}}}{\mathrm{VTEC}} = \int_{h_0}^{h_{\mathrm{ext}}} F_{\mathrm{RO}}(h)\,dh + h_s A \exp\left(-h_{\mathrm{ext}}/h_s\right), \quad (5)$$

the corresponding fractional contribution of the plasmasphere to the VTEC is given by

$$\mathrm{PL}_f = \frac{\mathrm{EC}_{\mathrm{pl}}}{\mathrm{VTEC}} = 1 - \mathrm{ION}_f\,. \quad (6)$$

The proposed method to separate the VTEC into $EC_{ion}$ and $EC_{pl}$ implicitly takes into account the interplay of the ionosphere-plasmasphere system by means of the best fit parameters achieved with the fitting function $F_{ext}(h)$. In particular, since these parameters are directly linked to the value of the UTH (see *González-Casado et al.* [2013] and the comments after equation (A3)), the method does not require the use of the specific value of the UTH (or any other characteristic boundary) to separate the ionosphere and the plasmasphere. Moreover, contrary to other studies based on the use of observations taken from a nearly constant satellite altitude, the results obtained in the present study will not be linked to the particular satellite altitude from which the RO measurements were taken. In fact, as it is shown in Appendix A, the topside ionosphere contribution to $EC_{ion}$ (above $h_{ext}$) derived with our method will never differ in more than 14% from the one calculated using the UTH as the boundary between the ionosphere and the plasmasphere. However, when this topside contribution is directly derived from the integrated electron density below the LEO satellite altitude, if $h_{LEO}$ is higher than the UTH, then the result can overestimate the actual topside contribution to $EC_{ion}$ by about 40% for the typical altitude of CF3 satellites. This overestimate is even greater for increasing values of $h_{LEO}$ (see Appendix A), giving rise to a significant underestimate of $EC_{pl}$.

On the other hand, the present method is not affected by the complications of using direct measurements from POD antennae (described in section 1), whereas RO measurements provide substantially greater coverage and better sampling of the electron content for different LTs and geographic locations in less time than POD observations. This is illustrated in Figure 2, where the red points show the trajectories in the LT versus latitude plane followed by the four satellites available from the CF3 constellation over two days (273 and 275) of 2007, while the green points indicate the corresponding position in that plane associated with the various ROs observed during the same days. POD antennae observations are essentially limited to points just over the satellite trajectories (which remain nearly the same after 2 days). In contrast, during the same period of time, RO observations will cover a significantly wider range of LTs and latitudes.

## 3. Observations and Data Sample

The CF3 constellation consists of six satellites that measure GPS signals during ROs. For the present study, the observations considered were from one fixed day per week during 2007, that is, 53 days evenly distributed throughout the year. RO-retrieved electron density profiles that did not extend upward beyond 700 km were discarded from the sample. Under these conditions, measurements from only four satellites of the CF3 constellation were included, but nevertheless, more than 60,000 electron density profiles were finally calculated after processing raw data from the COSMIC Data Analysis and Archive Center (CDAAC). As illustrated in Figure 2, the geographic locations of the orbits of the CF3 satellites change slowly from day to day. Using data from one fixed day per week avoids the accumulation of redundant data while providing reasonably dense coverage of all geographic locations around the globe, allowing a nearly worldwide analysis of the ionospheric

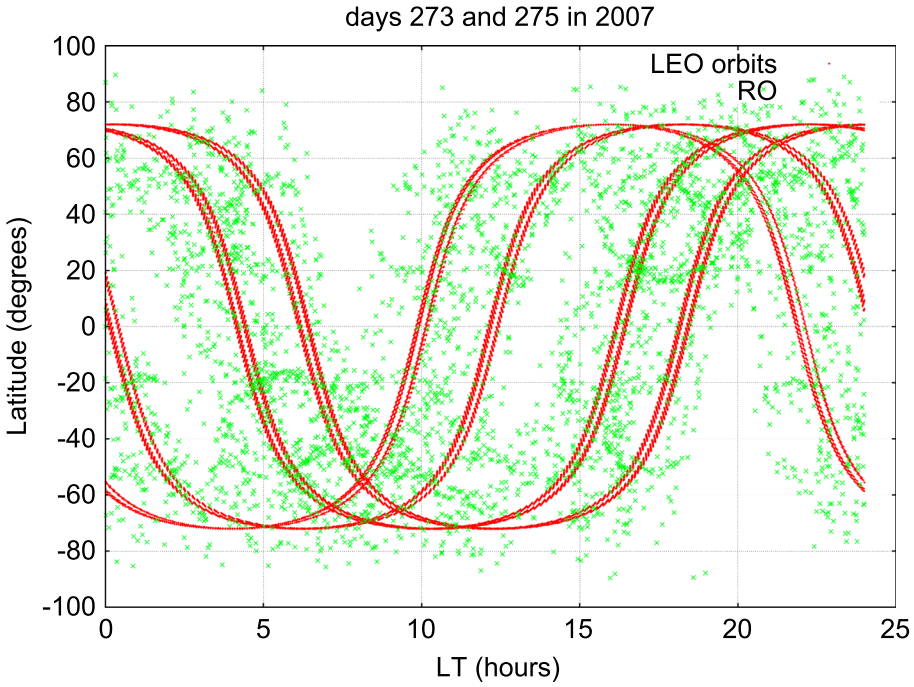


**Figure 2.** Red crosses: coordinates of the different satellites of the CF3 constellation in the latitude versus local time plane during the days 273 and 275 of year 2007. Green crosses: coordinates representative of the different radio occultations observed by the CF3 constellation during the same days.

and plasmaspheric electron contents for 2007. This year was part of a particularly long and deep solar minimum, lasting over 4 years. Specifically, during 2007, the 10.7 cm solar flux index $F_{10.7}$ was always smaller than 95 solar flux units, and it reached values over 80 less than 20% of the time. Additionally, periods of strong geomagnetic activity were very scarce in 2007, values of the magnetic activity index *Kp* greater than 4 rarely occurred during the days included in our sample, and the duration of such events was short.

All the electron density profiles were calculated using the IAT method, which requires the use of VTEC values to account for horizontal gradients in the electron content. The VTEC measurements were extracted from the GIM-TEC maps provided by IGS [see *Hernández-Pajares et al.*, 2009, and references therein]. For each RO-retrieved electron density profile from our sample, the fractional quantities $ION_f$ and $PL_f$ were first calculated according to equations (5) and (6), respectively. Subsequently, any value of the VTEC within the range of longitudes and latitudes covered by the RO could be used to derive the values of the ionospheric and plasmaspheric electron contents, $EC_{ion}$ and $EC_{pl}$, respectively, at the given geographic location. In the present study, we have used the VTEC values calculated at the geographic location of the tangent point of the GPS-LEO ray measured at the altitude of the $F_2$ layer peak of the electron density profile considered. The final sample contains approximately 60,000 pairs of measurements of $EC_{ion}$ and $EC_{pl}$ (and the respective fractional quantities). In the following sections this sample will be used to assess the performance of our method and to analyze the main dependencies (for different geomagnetic latitudes, LTs, and seasons of the year) of the ionospheric and plasmaspheric electron content.

## 4. LT and Seasonal Variations of the Ionosphere-Plasmasphere System

LT and seasonal variations in the ionosphere-plasmasphere system, particularly the annual, semiannual, and winter anomalies, have been analyzed in a number of previous studies [e.g., *Natali and Meza*, 2010; *Pedatella et al.*, 2011; *Lee et al.*, 2011; *Nanan et al.*, 2012; *Lee et al.*, 2013]. The impact of these anomalies in the plasmasphere has also been explored using both models and observations [*Pedatella el al.*, 2011; *Lee et al.*, 2013]. The results of these studies provide a reference that can be used to test the results obtained with the methodology presented in section 2. For a detailed description of the annual, semiannual, and winter (or seasonal) anomalies, see, for instance, *Natali and Meza* [2011].

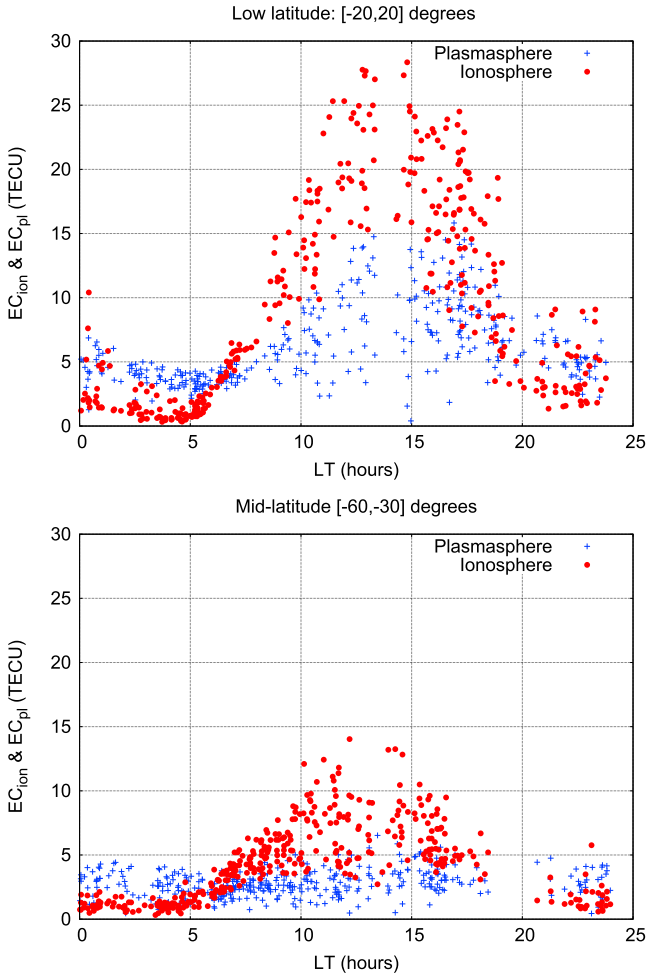


**Figure 3.** The different values of the electron content in the ionosphere and plasmasphere calculated from our sample of ROs during the day 274 of 2007. (top) Geomagnetic latitudes around the equator. (bottom) Intermediate geomagnetic latitudes in the Southern Hemisphere.

The electron content variations associated with the various anomalies depend on solar and magnetic activity and may be different in each Earth hemisphere. For example, a recent study by *Nanan et al.* [2012], using results from the Sheffield University Plasmasphere Ionosphere Model (SUPIM) model and CF3 observations, has reported the disappearance (and even the reversal) of the winter anomaly during the last solar minimum. On the other hand, analysis of GIM-TEC maps at different phases of solar activity shows that the amplitude of the variations caused by the semiannual anomaly can be 3 times larger during high solar activity than during low solar activity [*Natali and Meza*, 2010, 2011]. In relation to this, we recall that the data used in the present study correspond to a period of time of quite low solar and geomagnetic activity.

A preliminary examination of the LT variation of $EC_{ion}$ and $EC_{pl}$ for an individual day of our sample (day 274 of 2007) is presented in Figure 3. To minimize seasonal effects in the results, they are presented for a latitudinal band of $\pm 20°$ around the geomagnetic equator (Figure 3, top) and for geomagnetic latitudes between 30 and 60° in the Southern Hemisphere (Figure 3, bottom). One can observe that the dispersion in the results during the period of a few hours around sunrise (which occurs approximately at 5:00 LT) is significantly smaller than for the rest of the daytime and evening periods. In particular, the development of the daytime *F* layer can be unambiguously traced by the LT variation of the ionospheric electron content. Similarly, the increase of $EC_{pl}$ in the equatorial region a few hours after the raising of $EC_{ion}$ in the midlatitude ionosphere can be clearly observed. On the contrary, the values of the plasmaspheric electron content at midlatitudes remain nearly constant during the day with a very low dispersion, not greater than 1–2 TECU. Despite the dispersion of the results observed in Figure 3 around midday (mainly indicating latitudinal effects), one can clearly distinguish the different LT variations at low and intermediate geomagnetic latitudes of both $EC_{ion}$ and $EC_{pl}$.

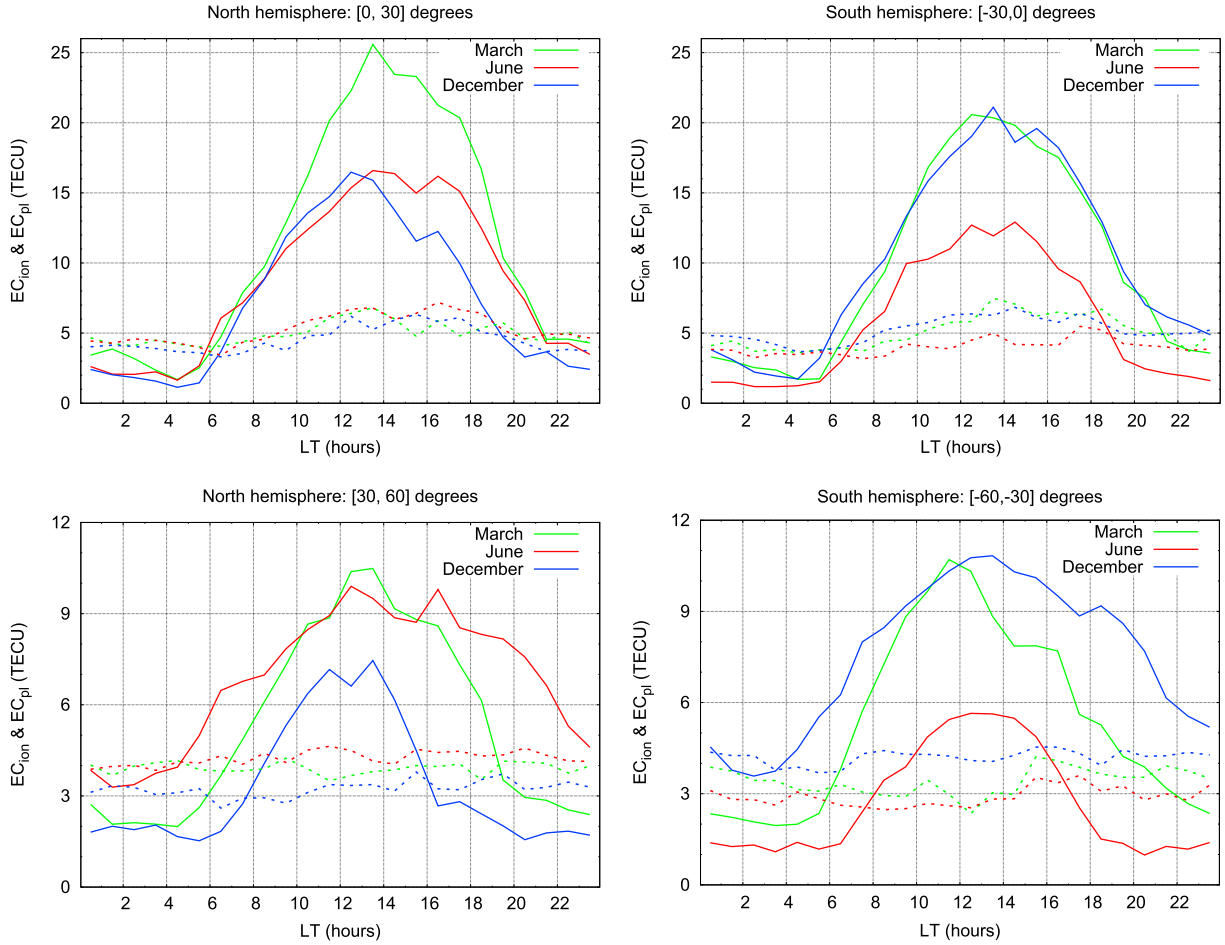


**Figure 4.** The LT variation of the mean electron content in the ionosphere (solid lines) and the plasmasphere (dotted lines) for low and intermediate geomagnetic latitudes in each hemisphere during the June and December solstices and the March equinox in 2007.

The mean electron contents of the ionosphere and the plasmasphere during the solstices and the spring equinox are represented in Figure 4, for the northern and southern geomagnetic hemispheres (left and right columns, respectively) and for low (top row) and intermediate (bottom row) geomagnetic latitudes. The mean values of $EC_{ion}$ and $EC_{pl}$ have been calculated at 1 h intervals over three periods of time centered on the June solstice, the December solstice, and the March equinox, each period covering 36 days (i.e., 6 days of data from our sample). In general, one can observe that the winter anomaly has disappeared in the ionosphere (solid lines) and also cannot be seen in the plasmasphere (dotted lines). The complete reversal of the winter anomaly is clearly observed at midlatitudes in the two hemispheres, the electron content during the local summer solstice being systematically greater than that during the local winter solstice. For low geomagnetic latitudes, the reversal of the winter anomaly can also be observed in the Southern Hemisphere, but only during the afternoon-evening in the Northern Hemisphere. Finally, Figure 4 shows that the difference between the local summer and local winter values of both $EC_{ion}$ and $EC_{pl}$ is larger in the Southern than in the Northern Hemisphere in the two latitudinal bands analyzed. These results are in agreement with previous studies based on ROs from the CF3 constellation and model calculations for the last solar minimum period [*Lee et al.*, 2011; *Nanan et al.*, 2012].

On the other hand, in Figure 4 it is also interesting to observe the existence of a clear hemispheric asymmetry in the midday values of $EC_{ion}$ at low geomagnetic latitudes during the March equinox. The semiannual anomaly in the equatorial ionosphere is much more prominent in the Northern than the Southern Hemisphere. A similar asymmetry has been reported from model calculations and also from the peak electron density and the TEC calculated from CF3 data during 2008 [*Nanan et al.*, 2012]. According to *Nanan et al.* [2012], this asymmetry is observed for deep solar minimum conditions and is associated with neutral winds that during the March equinox are more equatorward in the Northern Hemisphere.

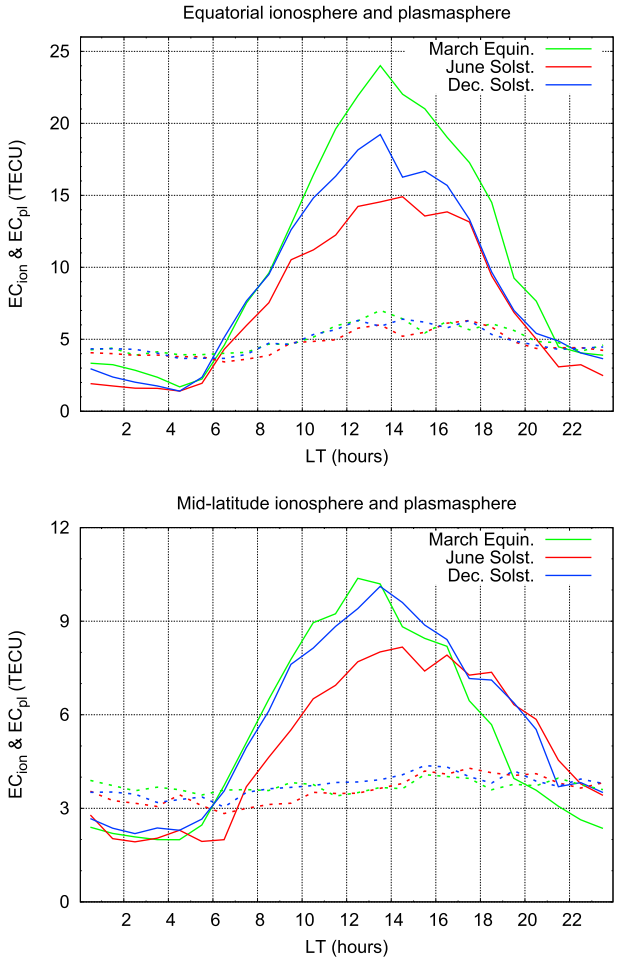


**Figure 5.** The LT variation of the mean electron content contributed by the ionosphere (solid lines) and the plasmasphere (dotted lines) during the June and December solstices and the March equinox in 2007. (top) Results from ROs in the geomagnetic latitude range (−30°, 30°). (bottom) Results from ROs in the geomagnetic latitude range from 30° to 60° in the Northern and Southern Hemispheres.

Figure 5 shows the same kind of study as presented in Figure 4 but without discriminating between the two hemispheres. The annual and semiannual anomalies can be observed in the ionospheric electron content (solid lines) particularly around noon as expected. For low geomagnetic latitudes $EC_{ion}$ is greater for the March equinox than for the December solstice (semiannual anomaly) from nearly 10:00 LT till the evening, while $EC_{ion}$ is greater for the December solstice than for the June one (annual anomaly) between 8:00 and 16:00 LT. The annual anomaly can also be observed for a similar time interval at midlatitudes, whereas the semiannual anomaly is less prominent and appears during a shorter period of time.

Previous studies [e.g., *Menk et al.*, 2012; *Lee et al.*, 2013] have shown the existence of an annual anomaly in the plasmasphere that is essentially observed in the range of longitudes covering the South American sector. In order to confirm this, the plasmaspheric electron content has been represented as a function of longitude in Figure 6. In this figure, the mean electron content of the equatorial plasmasphere during day and night periods has been calculated using intervals of 15° in longitude. One can observe the existence of an annual anomaly that has the greatest significance in the South American sector (longitudes from 200° to 300°). Moreover, according to Figure 6, the ratio between the December and June electron contents in that sector of longitudes is in the range of 1.5 to 2.0, in agreement with previous results [*Menk et al.*, 2012; *Lee et al.*, 2013]. Thus, we conclude that during the period of low solar activity analyzed in our study, the annual anomaly is simultaneously present in the ionosphere and the plasmasphere in the range of longitudes covering the South American sector, while this is not the case for the semiannual anomaly.

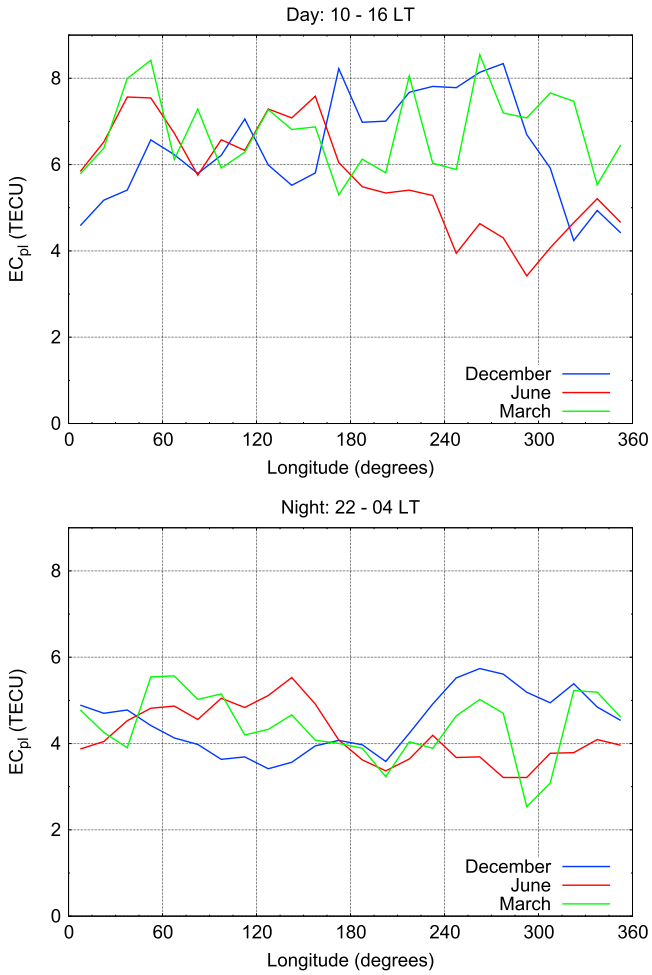


**Figure 6.** Longitudinal variation of the plasmaspheric electron content during the solstices and the March equinox for a latitudinal band of ±20° around the geomagnetic equator.

The ionospheric and plasmaspheric electron contents represented in Figures 3–5 show that during the night and especially in the few hours before sunrise the plasmasphere has a greater electron content than the ionosphere, which is broadly consistent with previous results [e.g., *Jee et al.*, 2010; *Lee et al.*, 2013]. Focusing on the LT variation in the plasmasphere, it is interesting to observe that the low-latitude plasmaspheric electron content shows a diurnal variation more or less similar to that seen in the ionosphere, but with a certain delay. In contrast, no significant LT variations are observed in the midlatitude plasmasphere. More specifically, the low-latitude plasmaspheric electron content starts increasing between 8:00 and 10:00 LT, a few hours after the enhancement of the midlatitude ionospheric electron content. The growth of $EC_{ion}$ after sunrise is triggered by the photoionization from sunlight and clearly traces the process of development of the daytime ionosphere over a few hours. However, very little ionization occurs in the plasmasphere, and hence, for undisturbed solar and geomagnetic periods (as it is the case for our data sample), the increase of $EC_{pl}$ beginning a few hours after sunrise could be related with the upward plasma flow that during the morning-midday period goes from the midlatitude ionosphere to the equatorial plasmasphere following the geomagnetic field lines. This has been recognized as an important mechanism feeding the daytime electron content in the equatorial plasmasphere [e.g., *Jee et al.*, 2005; *Lee et al.*, 2013].

## 5. Analysis of the Ionospheric Fractional Electron Content

The results presented in Figures 4 and 5 show that $EC_{ion}$ undergoes substantial variations over different periods of the year as well as between different geomagnetic latitudes, particularly around midday. Since $ION_f$ is a fractional quantity (represents the ionospheric electron content normalized to the VTEC), it can be more

adequate to characterize electron content variations of the ionosphere-plasmasphere system, regardless of the season of the year or the geomagnetic latitude considered. The variations of $ION_f$ will be, in general, mostly determined by changes in the ionospheric electron content, since $EC_{ion}$ is affected by significantly larger variations than $EC_{pl}$. For example, the difference between the midday and midnight values of the electron content in the plasmasphere is about 1 order of magnitude smaller than in the ionosphere. Similarly, seasonal and latitudinal variations in the ionosphere are much more significant than in the plasmasphere (see Figures 3 to 5).

### 5.1. Comparison With a Two-Layer Ionospheric Model

A quantitative validation of the results obtained for $ION_f$ from our methodology has been performed using a two-layer ionosphere-plasmasphere model as a reference. This two-layer model is employed in radio navigation applications for precise GNSS-based positioning, achieving positioning errors of the order of 10 cm or less [*Rovira-Garcia et al.*, 2014, 2015]. Such a low level of error requires a precision of model-provided ionospheric corrections of the order of 1 TECU. As shown in *Juan et al.* [2012], this accuracy in the ionospheric model is obtained thanks to processing ionospheric-free GNSS measurements in combination with a methodology for carrier phase ambiguity fixing. Unlike other ionospheric models based on a single layer at a fixed height, the present model uses a two-layer approach: a bottom layer accounting for the GNSS signal delays from the ionosphere and a top layer to account for the corresponding contribution from the plasmasphere. The altitude of the bottom layer is set at a value of 270 km, while an altitude of 1600 km is assumed for the top layer. Then, the measurements of the slant TEC obtained by GPS receivers from the IGS network of ground stations can be used, for instance, as input to the model, which delivers the resulting estimates of $EC_{ion}$ and $EC_{pl}$ at the different locations covered by the network. In thoroughly sounded regions (such as Europe and North America) there are sufficient data to solve the model equations with the required accuracy to obtain a reliable solution for the two layers separately [*Juan et al.*, 2012]. A direct calculation of the TEC from the ground to GPS satellite altitudes can be performed by adding the values of $EC_{ion}$ and $EC_{pl}$ derived from the two-layer model, or alternatively, the fractional electron content from the ionosphere can be evaluated from the ratio $EC_{ion}/(EC_{ion}+EC_{pl})$ and, subsequently, used as a reference to test the results independently obtained by means of the methodology described in section 2.

In Figure 7, the values of $ION_f$ derived from the two-layer model (red crosses) and calculated from our sample of ROs (blue crosses) can be directly compared. The ROs were selected in four different periods of 2007 with a time interval between two consecutive periods of approximately 10 weeks to ensure that the physical conditions of the ionosphere were significantly different in each period. The two-layer model calculations were performed for 1 day per period, more or less intermediate within each of the day intervals (see on top of each graph in Figure 7). The results presented were derived for a range of intermediate geomagnetic latitudes between 30 and 50° and for a range of longitudes from 0 to 60°, approximately corresponding to the European region, where a dense network of ground IGS stations exists. From Figure 7, one can see that there is good agreement between the LT variations of observations and model results, the main trends observed for the different periods of the year considered being similarly well reproduced. For the different periods of the year analyzed, the enhancement of $ION_f$ (in both the RO data and the model results) approximately coincides with the sunrise LT (indicated by a thick solid line in the graphs). During the hours preceding sunrise, the contribution of the ionosphere to the VTEC reaches a minimum while that of the plasmasphere peaks. During the morning, the situation reverses and the ionosphere then provides the greatest contribution to the VTEC, reaching a maximum around midday. Finally, unlike the results presented in Figures 4 and 5, where a large variation can be seen in the midday values of $EC_{ion}$ along the year, the four graphs presented in Figure 7 indicate that the typical value of $ION_f$ observed around midday is similar in the four periods of the year analyzed.

### 5.2. LT, Seasonal, and Geomagnetic Latitude Variations

The LT, summer/winter, and geomagnetic latitude variations of $ION_f$ calculated from our data sample are shown in Figure 8, where three different geomagnetic latitude bands have been considered: equatorial or low latitude (from 0 to 30° in each hemisphere, top row), midlatitude (from 30 to 60° in each hemisphere, middle row), and high latitude (from 60 to 90° in each hemisphere, bottom row). The results are presented separately in the Northern and Southern Hemisphere bands (red and blue points, respectively) for local summer and local winter (Figure 8, left and right columns, respectively). After binning the individual values of $ION_f$ into intervals of 1 h, the mean values were calculated for each bin and have also been represented in Figure 8 (solid lines). In general, only small differences are seen in the mean values of $ION_f$ between Northern and Southern Hemispheres. A much more outstanding feature observed in the different graphs in Figure 8 is that the

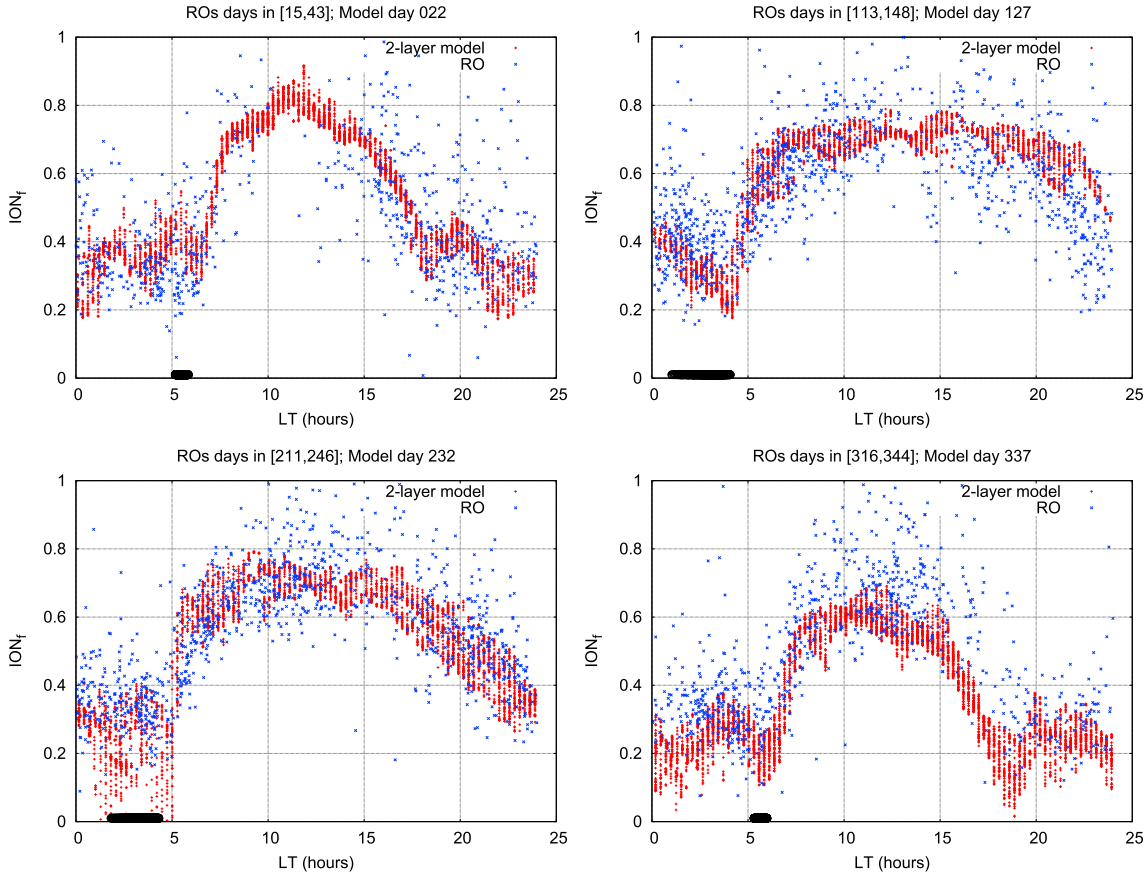


**Figure 7.** Comparison of the local time variation of the fractional electron content in the ionosphere, $ION_f$, during four different periods of 2007. Blue crosses: results from our sample of RO-retrieved electron density profiles corresponding to the period of the year indicated on top of each graph. Red crosses: results obtained from the two-layer ionospheric model described in the text for the interval of longitudes approximately covering the European region and using data from one intermediate day within the interval used for the observations (see on top of each graph). The black thick line over the *x* axis indicates the range of sunrise LTs corresponding to the period of the year covered by the samples used in each graph.

maximum mean value reached by $ION_f$ during the 24 h period is approximately the same in all cases (about 0.7) and occurs around noon, independently of the geomagnetic latitude range considered and for both summer and winter. This implies a nearly constant minimum value of $PL_f$ at the same time of the day and, consequently, an approximately constant proportion between the ionospheric and the plasmaspheric electron contents around noon along the year, regardless of the geomagnetic latitude. This proportionality indicates the existence of a significant coupling between the electron contents in the ionosphere and the plasmasphere during 2007.

On the other hand, Figure 8 shows that for low and intermediate geomagnetic latitudes the plasmasphere has a greater significance than the ionosphere during the night, particularly before sunrise and in winter, when it typically contributes from nearly 75% to as much as 80% of the VTEC around the geomagnetic equator. The lowest value of $ION_f$ during the 24 h period occurs just before sunrise and becomes smaller as the latitude decreases. This could be due to the effect of the $\mathbf{E} \times \mathbf{B}$ drift at low latitudes. During the nighttime, the downward drift reduces the equatorial ion density in the ionosphere, while during the daytime the upward drift enhances the ion density. In this way, a larger contrast between the day and night $ION_f$ values should be expected for low latitudes than for middle and high latitudes, as observed in Figure 8. Another effect that may contribute to values of $ION_f$ around the geomagnetic equator being lower than at midlatitudes during the night is the downward plasma flux from the equatorial plasmasphere toward the midlatitude ionosphere. This plasma flux enhances the presunrise values of $ION_f$ at intermediate geomagnetic latitudes more significantly than in the equatorial region.

Several characteristics of the regular ionospheric density variations can be clearly observed from the $ION_f$ results. For example, the differences in sunrise and sunset time between the two seasons analyzed are clearly

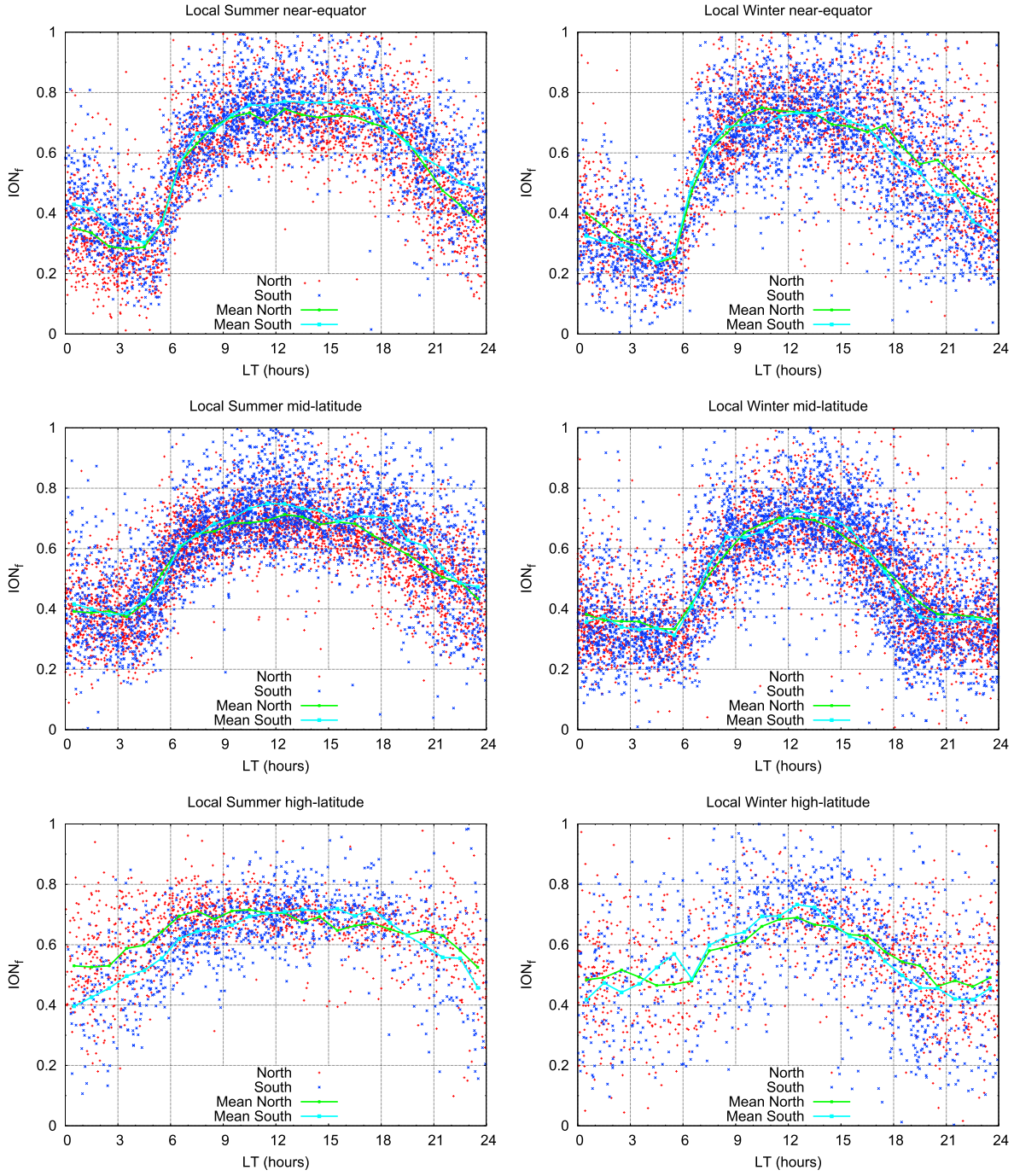


**Figure 8.** The fractional electron content in the ionosphere, $ION_f$, as a function of LT during (left column) local summer and (right column) local winter. Red and blue points correspond to individual values from our sample measured in Northern and Southern Hemispheres, respectively. (top row) Geomagnetic latitudes in (0°, 30°) in each hemisphere. (middle row) Geomagnetic latitudes in (30°, 60°) in each hemisphere. (bottom row) Geomagnetic latitudes greater than 60° in each hemisphere. The solid lines show the mean values calculated in intervals of 1 h from data on each hemisphere: northern (green) and southern (cyan).

noticeable in the solid curves in Figure 8, particularly for intermediate and high latitudes. The longer nights in winter will produce presunrise values of $ION_f$ which are slightly lower in winter than in summer as it is observed when comparing the left and right columns in Figure 8. Finally, the slope of the LT variation of $ION_f$ after sunrise has a marked latitudinal dependence which is very similar between the two seasons of the year analyzed. After sunrise the solar zenith angle decreases faster near the equator than at higher latitudes. For this reason, during the first hours after sunrise the effects of the photoionization from the Sun will be noticeable

near the equator faster than at middle and high latitudes. Consequently, one should expect an increase of the characteristic timescale of recovering of the daytime ionosphere with the geographic latitude, for both summer and winter. Although in Figure 8 the data are grouped within intervals of geomagnetic latitude, the effect can still be observed looking at the different rows in this figure.

## 6. Summary and Conclusions

A method based on RO measurements that allows calculation of the electron content in the ionosphere and the plasmasphere has been presented. The method self-consistently combines the IAT inversion technique for electron density retrieval, ground measurements of the VTEC, and adequate modeling of the topside ionosphere electron density. In this way, the ionospheric and plasmaspheric electron contents can be derived without relying on a fixed altitude to separate them. Applying this method to RO measurements from the CF3 satellite constellation and GIM-TEC maps from IGS, a global analysis of the contributions to the VTEC arising from the plasmasphere and the ionosphere has been performed for 2007, a year of low solar and geomagnetic activity. Hence, our conclusions are representative of this type of quiet period.

The present study has demonstrated that using only ionospheric electron density profiles derived from ROs is not sufficient to account for the VTEC, since such an approach systematically neglects the contribution of the plasmasphere, which in general is significant and can even be the main contribution to the VTEC, particularly before dawn for low and intermediate geomagnetic latitudes.

The study of the climatology of the main ionospheric anomalies performed in section 4, considering the separate contributions to the VTEC, $EC_{ion}$, and $EC_{pl}$, has confirmed previous findings for the recent solar minimum period, namely, the disappearance of the winter anomaly, the existence of an annual anomaly not only in the ionosphere but also in the plasmasphere, specifically in the South American sector of longitudes, and finally the semiannual anomaly in the ionosphere being more prominent in the Northern than in the Southern Hemisphere.

Our results have also shown that the ionosphere develops more abruptly and from a lower level of fractional electron content as the geomagnetic latitude decreases, and in general, the shape of the LT variation of $ION_f$ and $PL_f$ is essentially modulated by the geomagnetic latitude and to a lesser extent by the season of the year. The minimum value of $ION_f$ (and the corresponding maximum value of $PL_f$) is achieved just before sunrise and depends on geomagnetic latitude and season of the year, while the maximum value of $ION_f$ (and the corresponding minimum value of $PL_f$) is typically the same for all ranges of geomagnetic latitudes considered and for both summer and winter periods, the maximum always being achieved around noon, when the ionosphere has reached the state of maximum ionization. Therefore, the ratio between the electron contents of the ionosphere and the plasmasphere around midday is found to be nearly constant implying a strong coupling between both systems once the ionosphere has fully developed. To our knowledge, this is the first time that this feature is observed, and consequently, it deserves a more detailed analysis in the future, particularly using a data sample covering periods of intermediate and high solar and geomagnetic activity.

Many of the trends that have been observed in the ionospheric fractional electron content require further analysis, but the methodology introduced in the present work certainly opens the possibility of conducting studies of the ionosphere-plasmasphere system at a global scale. This may ultimately lead to improvement in the modeling of this coupled system. Another future application is the construction of global maps of the ionospheric and plasmaspheric portions of the TEC, which could potentially be applied to improve the reliability of current GIM-TEC maps for their further use, for instance, in space-based navigation systems.

## Appendix A: The Topside Contribution to the Ionospheric Electron Content

Consider the ionospheric electron content calculated according to the method proposed in section 2 (hereafter referred to as the extrapolating method) and by means of the direct integration of the electron density profile, $N_e$, downward a fixed altitude $h_f$ (as it is normally the case for satellite measurements). Below $h_{ext}$, both methods will give exactly the same contribution to the ionospheric electron content. But for altitudes higher than $h_{ext}$, the topside contribution to the ionospheric electron content calculated with the extrapolating method is

$$EC_{ext} = VTEC \int_{h_{ext}}^{\infty} A e^{-h/h_s}\, dh = VTEC\, h_s\, A\, e^{-h_{ext}/h_s}. \quad (A1)$$

On the other hand, assuming that the best fit STIP model is an accurate representation of the electron density profile in the topside ionosphere, the direct integration of $N_e$ downward $h_f$ yields the following expression for the topside contribution:

$$\mathrm{EC}(h_f) = \mathrm{VTEC}\int_{h_{\mathrm{ext}}}^{h_f}(Ae^{-h/h_s}+B)\,\mathrm{d}h = \mathrm{VTEC}\left[h_sA\left(e^{-h_{\mathrm{ext}}/h_s}-e^{-h_f/h_s}\right)+B(h_f-h_{\mathrm{ext}})\right]. \tag{A2}$$

The relative difference between equations (A2) and (A1) is

$$\Delta_{\mathrm{EC}} = \frac{\mathrm{EC}(h_f)-\mathrm{EC}_{\mathrm{ext}}}{\mathrm{EC}_{\mathrm{ext}}} = -e^{-x}+xe^{-(h_u-h_{\mathrm{ext}})/h_s}, \tag{A3}$$

where $x = (h_f - h_{\mathrm{ext}})/h_s$ and $h_u$ is the UTH that has been introduced in equation (A3) by means of the relation $B = Ae^{-h_u/h_s}$, derived from the STIP model [see *González-Casado et al.*, 2013].

Taking $h_f$ equal to $h_u$, one gets $\Delta_{\mathrm{EC}} = (x-1)e^{-x}$, which is a function having a maximum value approximately equal to 0.14 at $x = 2$. In particular, since the typical value of $h_{\mathrm{ext}}$ is about 400 km for our data sample, if $h_u \geq 300$ km (or equivalently, $x \geq 0.75$), then $|\Delta_{\mathrm{EC}}| < 0.14$. Hence, the difference between using the extrapolating method or using the UTH to separate the ionosphere and the plasmasphere is always smaller than 14% when the topside ionospheric electron content is calculated.

However, when $h_f$ is different from the UTH the value of $\Delta_{\mathrm{EC}}$ can be significantly greater, particularly if $h_f > h_u$. For example, for low solar activity periods, the median value of $h_u$ can be between 600 and 650 km while the median value of $h_s$ is around 100 km [see, e.g., *González-Casado et al.*, 2013]. Hence, in the case of CF3 satellites, where $h_f$ is around 750 km, one gets values of $\Delta_{\mathrm{EC}}$ ranging from 25 to 45%. But in the case that $h_f$ is close to 1000 km or higher (as, for example, measurements from the Jason satellite), $\Delta_{\mathrm{EC}}$ will be greater than 80%. It must be noticed that such deviations are caused by the bottomside plasmaspheric electron content being included as part of the topside ionospheric electron content when the latter is calculated using a fixed altitude higher than the UTH. Consequently, not only the resulting value of $\mathrm{EC}_{\mathrm{ion}}$ will be overestimated but also the value of $\mathrm{EC}_{\mathrm{pl}}$ will be substantially underestimated, the magnitude of the deviations depending on the particular value of the UTH.

**Acknowledgments**

The authors would like to thank the University Corporation for Atmospheric Research, the National Space Organization in Taiwan, and CDAAC for making available the FORMOSAT-3/COSMIC constellation data (http://cdaac-www.cosmic.ucar.edu/cdaac/). We also thank the International GNSS Service for the availability of IONEX files that provided us with VTEC data (http://igscb.jpl.nasa.gov/components/dcnav/cddis_products_ionex.html). This work has been partially supported by the Spanish Ministry of Science and Innovation project CTM2010-21312-C03-02.

Alan Rodger thanks three anonymous reviewers for their assistance in evaluating this paper.

## References

Aponte, N., C. G. M. Brum, M. P. Sulzer, and S. A. González (2013), Measurements of the $O^+$ to $H^+$ transition height and ion temperatures in the lower topside ionosphere over Arecibo for equinox conditions during the 2008–2009 extreme solar minimum, *J. Geophys. Res. Space Physics*, *118*, 4465–4470, doi:10.1002/jgra.50416.

Aragon-Angel, A., M. Hernández-Pajares, J. M. Juan, and J. Sanz (2010), Improving the Abel transform inversion using bending angles from FORMOSAT-3/COSMIC, *GPS Solut.*, *14*, 23–33, doi:10.1007/s10291-009-0147-y.

Aragon-Angel, A., Y. A. Liou, C. C. Lee, B. W. Reinisch, M. Hernández-Pajares, J. M. Juan, and J. Sanz (2011), Improvement of retrieved FORMOSAT-3/COSMIC electron densities validated by ionospheric sounder measurements at Jicamarca, *Radio Sci.*, *46*, RS5001, doi:10.1029/2010RS004578.

Belehaki, A., N. Jakowski, and B. W. Reinisch (2004), Plasmaspheric electron content derived from GPS TEC and digisonde ionograms, *Adv. Space Res.*, *33*, 833–837, doi:10.1016/j.asr.2003.07.008.

Garcia-Fernandez, M., M. Hernández-Pajares, J. M. Juan, and J. Sanz (2003), Improvement of ionospheric electron density estimation with GPSMET occultations using Abel inversion and VTEC information, *J. Geophys. Res.*, *108*(A9), 1338, doi:10.1029/2003JA009952.

González-Casado, G., J. M. Juan, M. Hernández-Pajares, and J. Sanz (2013), Two-component model of topside-ionosphere electron density profiles retrieved from Global Navigation Satellite Systems radio occultations, *J. Geophys. Res. Space Physics*, *118*, 7348–7359, doi:10.1002/2013JA019099.

Gulyaeva, T. L., X. Huang, and B. W. Reinisch (2002), Plasmaspheric extension of topside electron density profiles, *Adv. Space Res.*, *29*(6), 825–831.

Hernández-Pajares, M., J. M. Juan, and J. Sanz (2000), Improving the Abel inversion by adding ground GPS data to LEO radio occultation in ionospheric sounding, *Geophys. Res. Lett.*, *27*(16), 2473–2476.

Hernández-Pajares, M., J. M. Juan, J. Sanz, R. Orus, A. Garcia-Rigo, J. Feltens, A. Komjathy, S. C. Schaer, and A. Krankowski (2009), The IGS VTEC maps: A reliable source of ionospheric information since 1998, *J. Geod.*, *83*, 263–275, doi:10.1007/s00190-008-0266-1.

Jee, G., R. W. Schunk, and L. Scherliess (2005), On the sensitivity of total electron content (TEC) to upper atmospheric/ionospheric parameters, *J. Atmos. Sol. Terr. Phys.*, *67*, 1040–1052.

Jee, G., H.-B. Lee, Y. H. Kim, J.-K. Chung, and J. Cho (2010), Assessment of GPS global ionosphere maps (GIM) by comparison between CODE GIM and TOPEX/Jason TEC data: Ionospheric perspective, *J. Geophys. Res.*, *115*, A10319, doi:10.1029/2010JA015432.

Juan, J. M., et al. (2012), Enhanced precise point positioning for GNSS users, *IEEE Trans. Geosci. Remote Sens.*, *50*(10), 4213–4222, doi:10.1109/TGRS.2012.2189888.

Klimenko, M. V., V. V. Klimenko, I. E. Zakharenkova, and Iu. V. Cherniak (2014), The global morphology of the plasmaspheric electron content during northern winter 2009 based on GPS/COSMIC observation and GSM TIP model results, *Adv. Space Res.*, *55*(8), 2077–2085, doi:10.1016/j.asr.2014.06.027.

Lee, W. K., H. Kil, Y.-S. Kwak, Q. Wu, S. Cho, and J. U. Park (2011), The winter anomaly in the middle-latitude F region during the solar minimum period observed by the Constellation Observing System for Meteorology, Ionosphere, and Climate, *J. Geophys. Res.*, *116*, A02302, doi:10.1029/2010JA015815.

Lee, H.-B., G. Jee, Y. H. Kim, and J. S. Shim (2013), Characteristics of global plasmaspheric TEC in comparison with the ionosphere simultaneously observed by Jason-1 satellite, *J. Geophys. Res. Space Physics*, *118*, 935–946, doi:10.1002/jgra.50130.

Lunt, N., L. Kersley, G. J. Bishop, and A. J. Mazzella Jr. (1999), The contribution of the protonosphere to GPS total electron content: Experimental measurements, *Radio Sci.*, *34*(5), 1273–1280.

Makarevich, R. A., and M. J. Nicolls (2013), Statistical comparison of TEC derived from GPS and ISR observations at high latitudes, *Radio Sci.*, *48*, 441–452, doi:10.1002/rds.20055.

Menk, F. W., S. T. Ables, R. S. Grew, M. A. Clilverd, and B. R. Sandel (2012), The annual and longitudinal variations in plasmaspheric ion density, *J. Geophys. Res.*, *117*, A03215, doi:10.1029/2011JA017071.

Meza, A., C. Brunini, A. E. Gularte Scarone, and M. Mosert (2008), Analysis of a topside ionospheric model using GPS and ionosonde observables, *Adv. Space Res.*, *42*, 712–719, doi:10.1016/j.asr.2007.08.042.

Mosert, M., M. Gende, C. Brunini, R. Ezquer, and D. Altadill (2007), Comparisons of IRI TEC predictions with GPS and digisonde measurements at Ebro, *Adv. Space Res.*, *39*, 841–847, doi:10.1016/j.asr.2006.10.020.

Nanan, B., C. Y. Chen, P. K. Rajesh, J. Y. Liu, and G. J. Bailey (2012), Modeling and observations of the low latitude ionosphere-plasmasphere system at long deep solar minimum, *J. Geophys. Res.*, *117*, A08316, doi:10.1029/2012JA017846.

Natali, M. P., and A. Meza (2010), Annual and semiannual VTEC effects at low solar activity based on GPS observations at different geomagnetic latitudes, *J. Geophys. Res.*, *115*, D18106, doi:10.1029/2010JD014267.

Natali, M. P., and A. Meza (2011), Annual and semiannual variations of vertical total electron content during high solar activity based on GPS observations, *Ann. Geophys.*, *29*, 865–973, doi:10.5194/angeo-29-865-2011.

Pedatella, N. M., and K. M. Larson (2010), Routine determination of the plasmapause based on COSMIC GPS total electron content observations of the midlatitude trough, *J. Geophys. Res.*, *115*, A09301, doi:10.1029/2010JA015265.

Pedatella, N. M., J. M. Forbes, A. Maute, A. D. Richmond, T.-W. Fang, K. M. Larson, and G. Millward (2011), Longitudinal variations in the F region ionosphere and the topside ionosphere-plasmasphere: Observations and model simulations, *J. Geophys. Res.*, *116*, A12309, doi:10.1029/2011JA016600.

Rocken, C., Y. H. Kuo, W. Schreiner, D. Hunt, and S. Sokolovskiy (2000), COSMIC system description, *Terr. Atmos. Oceanic Sci.*, *11*(1), 21–52.

Rovira-Garcia, A., J. M. Juan, and J. Sanz (2014), A real-time world-wide ionospheric model for single and multi-frequency precise navigation, in *Proceedings of 27th International Technical Meeting of the Satellite Division of the Institute of Navigation (ION GNSS+ 2014), Tampa, Florida*, pp. 2533–2543, Inst. of Navig., Tampa, Florida, 8–12 Sept.

Rovira-Garcia, A., J. M. Juan, J. Sanz, and G. González-Casado (2015), A world-wide ionospheric model for fast precise point positioning, *IEEE Trans. Geosci. Remote Sens.*, *53*, 4596–4604, doi:10.1109/TGRS.2015.2402598.

Schreiner, W., C. Rocken, S. Sokolovskiy, S. Syndergaard, and D. Hun (2007), Estimates of the precision of GPS radio occultations from the COSMIC/FORMOSAT-3 mission, *Geophys. Res. Lett.*, *34*, L04808, doi:10.1029/2006GL027557.

Yizengaw, E., M. B. Moldwin, D. Galvan, B. A. Iijima, A. Komjathy, and A. J. Mannucci (2008), Global plasmaspheric TEC and its relative contribution to GPS TEC, *J. Atmos. Sol. Terr. Phys.*, *70*, 1541–1548, doi:10.1016/j.jastp.2008.04.022.

Yue, X., W. S. Schreiner, J. Lei, C. Rocken, Y.-H. Kuo, and W. Wan (2010), Climatology of ionospheric upper transition height derived from COSMIC satellites during the solar minimum of 2008, *J. Atmos. Sol. Terr. Phys.*, *72*, 1270–1274, doi:10.1016/j.jastp.2010.08.018.